I&EC research
Industrial & Engineering Chemistry Research

Article

pubs.acs.org/IECR

New Formulations of Ni-Containing Ceramic Papers to Enhance the Catalytic Performance for the Oxidative Dehydrogenation of Ethane

J. P. Bortolozzi, E. D. Banús, V. G. Milt, and E. E. Miro*

Instituto de Investigaciones en Catálisis y Petroquímica, INCAPE (FIQ, UNL-CONICET), Santiago del Estero 2829, (S3006BMF) Santa Fe, Argentina

ABSTRACT: Ceramic papers composed of silica−alumina fibers structured using colloidal suspensions as binders constitute interesting materials to be used as flexible supports of catalytic materials. The deposition of Ni as the active ingredient together with Zr or Ce promoters resulted in active and selective structured catalysts for the oxidative dehydrogenation of ethane; these structured catalysts also exhibited acceptable mechanical properties. The employed binder agents (nanoparticles of ceria, zirconia, or yttria-stabilized zirconia) homogeneously covered the fiber surface, contributing to the dual function of building a three-dimensional arrangement and favoring the anchoring of the catalytic formulations. The prepared papers showed nickel oxide as the active phase. The incorporation of cerium or zirconium as promoters enhanced the catalytic properties. The former element mainly produced an increase in ethane conversion, whereas the latter markedly improved ethylene selectivity. In both cases, an ethylene productivity was obtained in the promoted systems which was higher than that in the unpromoted samples. It is likely that the formation of the solid solutions Ni−Ce−O and Ni−Zr−O, as suggested by X-ray diffraction and laser Raman spectroscopy analyses, plays an important role in these effects. The best catalyst was the one containing nickel as the active phase, Ce as the promoter, and ZrY as the binder agent, for which ethylene productivity at 400 °C was ca. 513 g ethylene/(kg_{cat} h). The binder agent addition was necessary to join the fibers, thus improving the mechanical properties of the papers, but they also affected the catalytic performance through the coverage of ceramic fibers and the resulting interaction with the catalytic compounds. The performed tensile index tests showed that the colloidal suspension of ceria produced papers with mechanical properties better than those of zirconia or zirconia−yttria because they exhibited greater resistance and flexibility.

1. INTRODUCTION

At present, light olefins such as ethylene are of great industrial interest and, consequently, their demand is growing quickly. Ethylene is used as a valuable intermediary in the synthesis of different compounds, e.g., polymers and fibers. It is produced by the steam cracking of certain petroleum fractions such as naphtha or ethane. However, this process is one of the most energy-consuming in the petrochemical industry. With the aim of investigating substitute processes that require less energy and that operate at less severe conditions, some alternative routes are under study. The production of ethylene through the catalytic oxidative dehydrogenation of ethane (ODE) is an attractive process because it is simple and the reactions involved are exothermic, thus leading to a better energy balance.[1]

It is well-known that nickel oxide is active for converting ethane to ethylene but shows very low selectivity.[2−4] Heracleous et al.[5,6] studied alumina-supported nickel and bulk NiO catalysts applied to this reaction with the addition of a variety of promoters. They concluded that the presence of alumina modifies the electronic properties of nickel oxide making it more selective toward ethylene. In addition, the presence of niobium significantly enhances the catalytic performance in the supported catalysts as well as in the nickel oxide bulk forms.

Solsona et al.[7] also studied powder-supported and bulk nickel oxide catalysts containing tungsten as promoter. When supported on alumina, the good catalytic performance could be related to the high dispersion of NiO, which could prevent the formation of nonselective sites. For bulk formulations, it was established that the nature of nickel active sites and their acidity determined the catalytic behavior.[8] In addition, cerium was also used as a favorable promoter because it improved the ethane conversion and selectivity to ethylene in powder catalysts. However, changes in the catalytic behavior depended on the catalyst composition.[9]

According to Wu et al., doping nickel oxide with zirconium affects the oxide reducibility and modifies the distribution of adsorbed oxygen species, thus influencing their catalytic performance in the ODE reaction.[10]

Going a step beyond catalyst design and taking into account a possible engineering application, Bortolozzi et al. tested alumina-supported catalysts over metallic[11,12] and ceramic[13] foams, exploiting the characteristic advantages of structured catalysts. In those previous studies, it was found that the addition of cobalt as promoter slightly improved the catalytic performance while the incorporation of cerium significantly enhanced the ethylene productivity, according to previously published results.[9] It was also shown that when the catalysts were deposited onto metallic substrates, both the activity and selectivity to ethylene changed, either by the nonhomogeneity in the concentrations of the active phases or by the presence of certain elements coming from the metallic foam.[11,12] Nevertheless, a higher efficiency could be obtained with Ni and Ni−

Received: August 8, 2014
Revised: October 17, 2014
Accepted: October 17, 2014
Published: October 17, 2014

dx.doi.org/10.1021/ie503154f | *Ind. Eng. Chem. Res.* 2014, 53, 17570−17579

Ce/alumina coated onto ceramic foams because the effect of the foreign components was negligible.[13]

In brief, the deposition of a catalytic formulation onto a suitable substrate has a positive effect on the ethylene productivity compared with powder forms and constitutes an interesting topic for further investigation. In this sense, a paperlike structure composed of a fibers network with interconnected porelike spaces could constitute an adequate environment that favors the effective diffusion of the reagents and products throughout the catalytic bed.[14−17] The heat transfer could also be enhanced, which is useful for exothermic-type reactions such as the oxidative dehydrogenation reactions.

Ceramic papers are commonly built as a blanket of alumina−silica fibers.[15] To increase the mechanical resistance, different binder agents are used, which allow the joining of the fibers and give stiffness and flexibility to the arrangement.

This kind of substrate has been used for many types of reactions such as catalytic combustion of soot;[14,15] steam reforming of hydrocarbons;[16,17] methane dry reforming;[18] toluene removal;[19] reduction of 4-nitrophenol;[20] selective catalytic reduction of NO_x with C_3H_6,[21] NH_3,[22] and CH_4;[23] and methanol reforming,[24] among others.

In a first and exploratory contribution, Ni and Ni−Ce catalysts were incorporated in these innovative substrates and tested in the ODE reaction, using colloidal alumina as binder agent. In terms of ethane conversion and ethylene productivity, an adequate performance with moderate selectivity could be obtained. The Ce/Ni = 0.17 atomic ratio was shown to be optimal for achieving the best ethylene yield of the tested systems.[25] It was found that alumina nanoparticles partially covered the ceramic fibers, not only helping to bind fibers but also anchoring catalytic components over them. With this idea in mind, the aim of this work was to further investigate the role of different materials used as promoters and binders (CeO_2, ZrO_2, and yttria-modified ZrO_2) to enhance catalytic and mechanical properties.

For that purpose, a series of ceramic papers were prepared with three different binders, i.e., colloidal suspensions (Nyacol) of cerium, zirconium, and zirconium−yttrium oxides, to improve their mechanical properties. On the other hand, cerium and zirconium nitrates were impregnated on the fibers as promoters of nickel, with the purpose of enhancing the catalytic activity and selectivity. Please note that the same materials, although introduced in different ways, were selected for enhancing both mechanical and catalytic properties.

The developed structured catalysts were characterized by different techniques and tested for their application in the oxidative dehydrogenation of ethane reaction. The mechanical properties and pressure drop of the catalytic ceramic papers were also evaluated.

2. EXPERIMENTAL SECTION

2.1. Synthesis of Ceramic Papers. For the ceramic paper preparation, two types of fibers were used: ceramic fibers (50 wt % SiO_2, 48 wt % Al_2O_3, 2 wt % impurities, from Carbo Ceramic) and cellulosic fibers, obtained by repulping an industrial blotting paper, produced from bleached softwood Kraft with slightly refined fibers. Before their use, ceramic fibers were elutriated, washed, and dried to both homogenize the size of the fibers and eliminate the soluble impurities. The energy-dispersive X-ray analysis performed after the purification stage showed that the remaining impurities were composed of iron and titanium and the total amount was lower than 1 wt %. It is worth mentioning that the presence of iron could result from the manufacturing process, while the presence of titanium is typical when aluminum is also present.

A papermaking technique with a dual polyelectrolyte retention system was adopted, which implied the use of cationic and anionic polymers. These polyelectrolytes generate a double layer of charged polymers on ceramic fibers and also generate bridges which join these fibers, thus increasing the retention of particles during the papermaking process.[26,27] The cationic polymer was polyvinyl amine (PVAm, LUREDUR PR 8095) from BASF, molecular weight 4×10^5 g/mol and charge density 4.5 mequiv/g, and the anionic polymer was polyacrylamide (A-PAM) from AQUATEC, molecular weight 10^4−10^5 g/mol and charge density 2.7 mequiv/g.

Commercial colloidal suspensions (Nyacol, 20 wt %) of CeO_2, ZrO_2, or Yttria-stabilized ZrO_2 were added as binders to provide mechanical strength to the final structure.

Ceramic papers were prepared by the above-mentioned papermaking technique. First, 1 L of NaCl (0.1 N) solution was stirred into a reactor with 66 mL of cationic polyelectrolyte Luredur. Then, ceramic fibers (10 g), the selected colloidal suspension (10 g), 42 mL of anionic polyelectrolyte A-PAM, and finally 1.5 g of cellulosic fiber were incorporated every 3 min under constant stirring. Using this suspension and following the standard SCAN method (SCAN-C 26:76 and SCAN-M 5:76), but applying double the usual pressure (37.5 kPa), a sheet was formed. The molded sheet (160 mm in diameter) was dried under controlled atmosphere (23 °C, 50% RH) for 24 h and finally calcined in air for 2 h at 550 °C, with a heating rate of 1 °C/min.

Ceramic papers thus obtained were denoted as PCe, PZr, or PZrY according to the colloidal suspension employed in the preparation procedure: ceria, zirconia, or yttria-stabilized zirconia, respectively. Figure 1 shows a schematic diagram with the sequence of the synthesis process.

2.2. Catalytic Component Incorporation. To prepare catalytic ceramic papers, ceramic paper sheets (PCe, PZr, or PZrY) were cut into 15 mm diameter discs. Solutions of $Ni(NO_3)_2$ (0.2 M), $Ce(NO_3)_3$ (0.2 M), and $Zr(NO_3)_4$ (0.2 M) or mixtures of them were used to incorporate the catalytic and promoter components. Ceramic paper discs were moistened up to saturation with the nickel nitrate solution or the mixed solution of nickel and cerium nitrates or nickel and zirconium nitrates; for the latter two cases, a Ce/Ni atomic ratio of 0.17[25] and a Zr/Ni atomic ratio of 0.11[10] were used. After the impregnated papers were dried at room temperature for 24 h, they were calcined in air at 500 °C for 2 h. The structured catalysts thus obtained were designated as NiX−PCe, NiX−PZr, or NiX−PZrY, where X, if applicable, indicates the promoter employed (cerium or zirconium).

2.3. Physicochemical Characterization. *2.3.1. X-ray Diffraction (XRD).* Crystalline phases were identified with a Shimadzu XD-D1 instrument using Cu Kα radiation at a scan rate of 2°/min, from 2θ = 20° to 80°. The ceramic paper pieces were supported in a special sample holder designed for the XRD analysis. The software package of the instrument was used for phase identification from the X-ray diffractograms. Crystallite sizes were estimated by the Scherrer equation, employing the main peaks (2θ) of each compound: 43.3° for NiO and 29.6° for CeO_2.

2.3.2. Laser Raman Spectroscopy (LRS). A Horiba Jobin Yvon LabRAM HR instrument was used. The excitation wavelength was 532.13 nm (Spectra Physics diode pump solid-

dx.doi.org/10.1021/ie503154f | Ind. Eng. Chem. Res. 2014, 53, 17570−17579

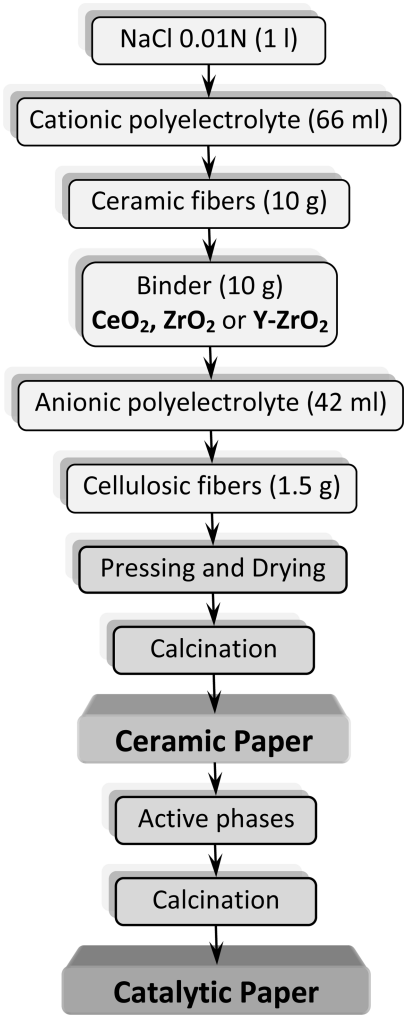

Figure 1. Scheme of catalytic ceramic paper preparation.

state laser with the power set at 30 mW). Several spectra were acquired for each sample.

2.3.3. Scanning Electron Microscopy (SEM). A JEOL JSM-35C electronic microscope was employed using an operation acceleration voltage of 20 kV. Samples were glued to the sample holder with Ag painting and then coated with a thin layer of Au to improve image quality.

2.3.4. Energy-Dispersive X-ray Analysis (EDX). The elemental chemical analysis was performed trying the X-ray spectra with the EDAX software. Semiquantitative results were obtained with the theoretical quantitative method (SEMIQ), which does not require standards. X-ray spectra were obtained with an acceleration voltage of 20 kV.

2.4. Mechanical Properties and Pressure Drop. The tensile strength and stiffness of the ceramic papers were determined in a universal test equipment (INSTRON 3344) with a load cell of 10 N, using the standard TAPPI T 576 pm-07 method to estimate the properties of tissue papers. Ceramic paper pieces of about 2 mm thickness, 50 mm width, and 70 mm length were evaluated, leaving a free length between grips of 50 mm.

To determine the permeability of the prepared ceramic papers as a measure of the resistance to the gas flow passage, a specific system developed by Tuler et al. was employed.[15] Briefly, it consists of a stainless steel cylinder inside which the ceramic paper discs were piled up. A wire mesh joined to one of the ends of the container acted as bed support. Its respective flange and bolts closed the vessel and a thermoplastic polymer sealed the joint. Ten catalytic ceramic papers were stacked to the experiments and Q/A versus $\Delta P/L$ curves were obtained by changing the inlet air pressure and measuring the permeated air flow. Q is the measured air flow (mL/s), A the flow area (243 mm^2), ΔP the pressure drop through the bed (bar), and L, the bed height (20 mm).

2.5. Catalytic Tests. The oxidative dehydrogenation of ethane was carried out in a flow system in the temperature range between 280 and 440 °C. The feed composition was 6% O_2 and 6% C_2H_6 with helium balance. Eight catalytic paper discs (ca. 15 mm in diameter) were stacked in the middle of a quartz reactor (Figure 2). The total mass of catalyst deposited

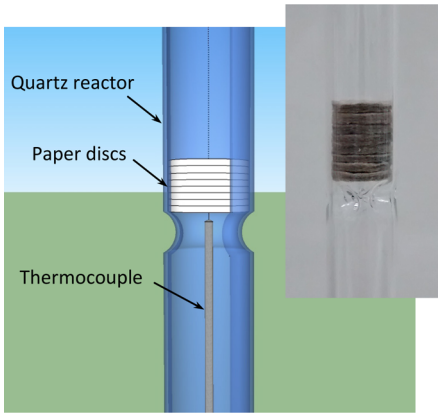

Figure 2. Scheme of catalytic ceramic papers disposed into the reactor. Inset: Picture of the structured systems ready for catalytic evaluation.

on the papers (nickel and promoter oxides, i.e., NiO, NiO–CeO_2, or NiO–ZrO_2) was ca. 65 mg. The standard W/F value used to compare the activity of the different catalysts was 0.08 g s/cm^3, where W refers to the above-mentioned total weight of the catalyst deposited on the paper fibers (as NiO + CeO_2 (or ZrO_2), if applicable) and F is the total flow rate. To analyze the relationship between selectivity and conversion at a constant temperature, a second set of experiments was carried out in which the W/F ratio was varied to achieve different conversion levels at 360 °C.

Reactants and products were analyzed with a Shimadzu GC 2014 gas chromatograph equipped with a packed column (HayeSep D). Closure of the carbon mass balance was 100 ± 3%. Carbon monoxide or other products were not detected in the product stream after the reaction. The total oxygen conversion never reached 100%. Under the experimental conditions used in the catalytic tests, the contribution of gas-phase reactions was negligible.

To evaluate the global catalytic behavior, the ethylene productivity by kilogram of catalyst was calculated at fixed temperatures (280, 400, and 440 °C) as follows:

$$P[g_{C_2H_4}/(kg_{cat}\ h)] = 28F_{C_2H_6}X_{C_2H_6}S_{C_2H_4}/W_{cat}$$

where 28 is the molecular mass of ethylene (g/mol), F the flow rate of ethane (mol/h), X the ethane conversion, S the selectivity to ethylene, and W_{cat} the mass of catalyst (nickel + promoter oxides; kg).

dx.doi.org/10.1021/ie503154f | Ind. Eng. Chem. Res. 2014, 53, 17570–17579

3. RESULTS AND DISCUSSION

3.1. Oxidative Dehydrogenation: Catalytic Performance and Ethylene Productivity. Figure 3 shows the ethane

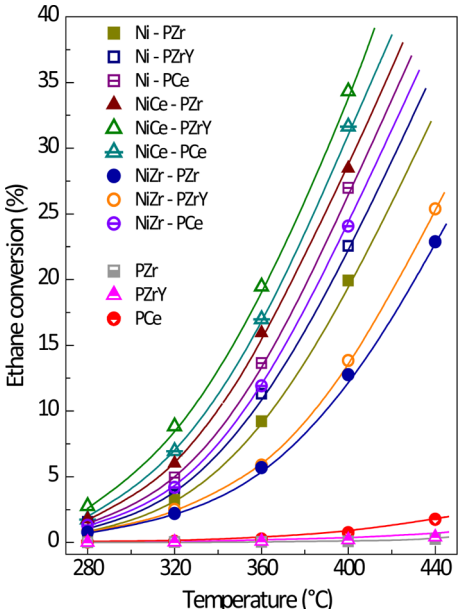

Figure 3. Ethane conversion curves for the different catalytic and bare papers (T, variable; W/F = 0.08 g s/cm^3).

conversion in the 280−440 °C range for the structured catalysts. Among the evaluated systems, the promoter-free catalytic papers exhibited an intermediate activity for the oxidative dehydrogenation of ethane. Even considering the very low W/F ratio used in the experiments (0.08 g s/cm^3), the systems showed measurable catalytic activity at temperatures as low as 280 °C.

As a general trend, the addition of cerium to the formulations significantly enhanced the activity. For example, the papers prepared with a yttria-stabilized zirconia binder (Ni−PZrY) showed a conversion improvement of around 100% at 280 °C after the addition of CeO_2 as promoter (NiCe−PZrY), whereas the conversion improvement was about 55% at 400 °C. In contrast, the addition of a zirconium promoter (NiZr−PZrY) produced a decrease in the ethane conversion, as compared with that of Ni−PZrY. Nevertheless, the zirconium-promoted formulations showed a reasonable conversion level of about 25% in the range of 410−440 °C.

It is clear that the binder agent has some influence on the catalytic activity because the same catalytic formulation deposited onto three different ceramic papers (prepared using the three different types of colloidal suspensions) led to different values of ethane conversion. This behavior is variable according to the system. For example, the Ni−PCe catalyst showed the highest activity among the free-promoter systems, whereas NiCe−PZrY displayed the highest conversions among the NiCe-containing papers. The NiCe−PCe paper contains Ce that comes from two sources of Ce: the binder agent and the promoter, whose amount affects the catalytic activity, as will be more carefully discussed with EDX results. However, it is worth mentioning that the optimal Ce/Ni ratio is around 0.17[25] and also that the cerium oxide by itself presents a very poor catalytic performance for the ODE reaction. This can explain the slightly lower ethane conversion observed for this formulation (NiCe−PCe) in comparison to that for NiCe−PZrY.

A set of experiments was performed to study the effect of W/F on both selectivity and productivity at constant temperature (360 °C), and Figure 4 displays the selectivity to ethylene at the

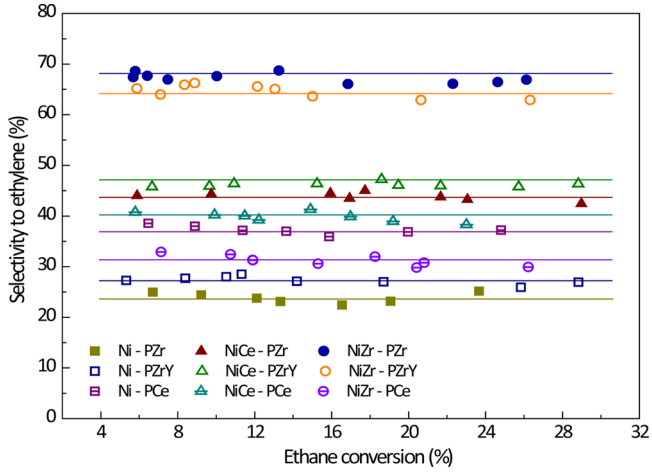

Figure 4. Ethylene selectivity at constant temperature (T = 360 °C; W/F, variable).

different ethane conversion values obtained. For all the systems studied, selectivity remains approximately constant as ethane conversion increases up to 30%. The almost flat tendency observed suggests that in the analyzed cases, carbon dioxide was formed by direct oxidation of ethane and not by the secondary reaction, i.e., the oxidation of ethylene did not occur to a significant extent.

As expected, nonpromoted Ni-containing papers showed the lowest selectivity among the evaluated systems. However, Ni−PCe presented the higher values between the nonpromoted samples, thus suggesting the evident interaction between the catalytic formulation and the binder agent employed, in agreement with the behavior observed in ethane conversion. This point will be further discussed below. In addition, a high dispersion of nickel on the cerium oxide coverage could be achieved, which also contributes to the enhanced ethylene selectivity.

On the other hand, the cerium-promoted systems exhibited intermediate selectivity values, whereas the zirconium-promoted papers showed the best selectivity values, around 70%, even up to an ethane conversion level of 26% for NiZr−PZr. The only exception was NiZr−PCe, which presented low selectivity, possibly because of the interaction between nickel and zirconium with cerium coming from the fiber coverage.

To evaluate the contribution of the studied substrates to catalytic activity, ceramic papers without active phases (PCe, PZr, and PZrY) were evaluated under the reaction conditions that were the same as those used for the catalytic papers. The ceramic paper prepared with colloidal ceria as binder agent (PCe) showed 1.7% of ethane conversion at 440 °C, whereas the other two papers (PZr and PZrY) showed a maximum conversion of 0.5% at the same temperature (Figure 3). Moreover, the selectivity toward ethylene was null for the three ceramic papers. Therefore, no active species for the oxidative dehydrogenation reaction were present in the bare ceramic papers.

dx.doi.org/10.1021/ie503154f | Ind. Eng. Chem. Res. 2014, 53, 17570−17579

In addition, as mentioned in the Experimental Section, homogeneous reactions did not occur, which was verified with the empty reactor tested under the selected conditions.

Ethylene productivity was calculated at both 280 and 400 °C, and the corresponding values are presented in Table 1. All prepared systems present high ethylene production rate even at the lowest temperature analyzed (Table 1). In general, the productivity was improved with the addition of both cerium and zirconium if compared with that of the unpromoted papers. The incorporation of cerium led to a marked increase of the ethylene productivity because of both better conversion and selectivity. The system NiCe−PZrY produced 53.3 g ethylene/(kg_{cat} h) at only 280 °C (Table 1), and at 400 °C, it reached 513.4 g ethylene/(kg_{cat} h), which represents a remarkable increment with respect to the corresponding unpromoted catalyst Ni−PZrY.

Table 1. Ethylene Productivity of the Catalytic Papers at Different Temperatures

	ethylene productivity (g ethylene/(kg_{cat} h))	
catalytic paper	280 °C	400 °C (440 °C)
Ni−PZr	8.4	152.4
Ni−PZrY	20.7	179.4
Ni−PCe	24.0	246.9
NiCe−PZr	33.8	395.6
NiCe−PZrY	53.3	513.4
NiCe−PCe	32.3	342.1
NiZr−PZr	19.6	274.1 (474.3)
NiZr−PZrY	21.8	305.0 (530.5)
NiZr−PCe	24.5	181.2

The moderate conversion achieved by zirconium-promoted papers (Figure 3) was compensated by their high selectivity (Figure 4), thus also reaching higher productivity than nonpromoted Ni-containing papers. If the productivity is calculated at 440 °C for NiZr−PZr and PZrY systems, the values obtained are close to that of NiCe−PZrY, which is, in terms of ethylene productivity, the best catalyst prepared (Table 1).

As previously mentioned, a different behavior was presented by NiZr−PCe, which showed the lowest ethylene production among the promoted catalysts, mainly caused by the intermediate conversion and low selectivity. The interaction of the three elements (Ni and Zr with Ce from the fiber coverage), in this case, was negative. Despite having the same components, NiZr−PCe and NiCe−PZr, the second shows twice the productivity of the first one. The different Ni/Zr and Ni/Ce ratios could be one of the causes of the difference in productivity. As will be later discussed, another explanation of this behavior could be the different morphologies, as seen by SEM. The possible formation of Ni−Zr−Ce solid solutions which contain more mobile oxygen species, thus affecting both conversion and selectivity, should not be discounted. The incorporation of nickel ions into the ceria and/or zirconia structures due to the fact that their ionic radius is slightly smaller than that of zirconium ions and cerium ions radii (0.72 Å for Zr^{4+} and 0.97 Å for Ce^{4+} versus 0.69 Å for Ni^{2+}) has been reported in the literature.[28] In addition, the substitution of some cerium ions by zirconium ions could produce a Ce−Zr solid solution that presents an enhanced oxygen storage capacity, which could be negative for the reaction under study because of their highly oxidative properties.[29,30] Nevertheless, a deeper study of the Ni−Zr−Ce combination seems to be necessary to shed light on this topic and to elucidate the reasons for this behavior, but such a study exceeds the scope of this work.

On the other hand, to obtain a first approach of their catalytic stability, all prepared systems were evaluated under reaction for more than 20 h. No significant differences were found on ethane conversion or on selectivity, which highlights the stability of the developed catalytic ceramic papers under time-on-stream.

3.2. Morphology and Chemical Composition of the Catalysts. The papermaking technique is a simple process that allowed us to obtain flexible, versatile, easy-to-handle ceramic papers. The addition of active phases permitted us to obtain catalytic papers that are resistant under the selected operating conditions. The reasons for these properties can be related to the morphology of the structures. All prepared papers showed an interconnected three-dimensional (3-D) network of ceramic fibers that remains after the combustion of cellulosic fibers during calcination. The porelike spaces vary from 10 to 100 μm approximately, thus offering an optimal media for the passage of a gas stream.

The morphology of the ceramic papers was similar in all cases, independent of the binder used (CeO_2, ZrO_2 or Y-ZrO_2) (Figure 5). The employment of CeO_2 colloidal suspension

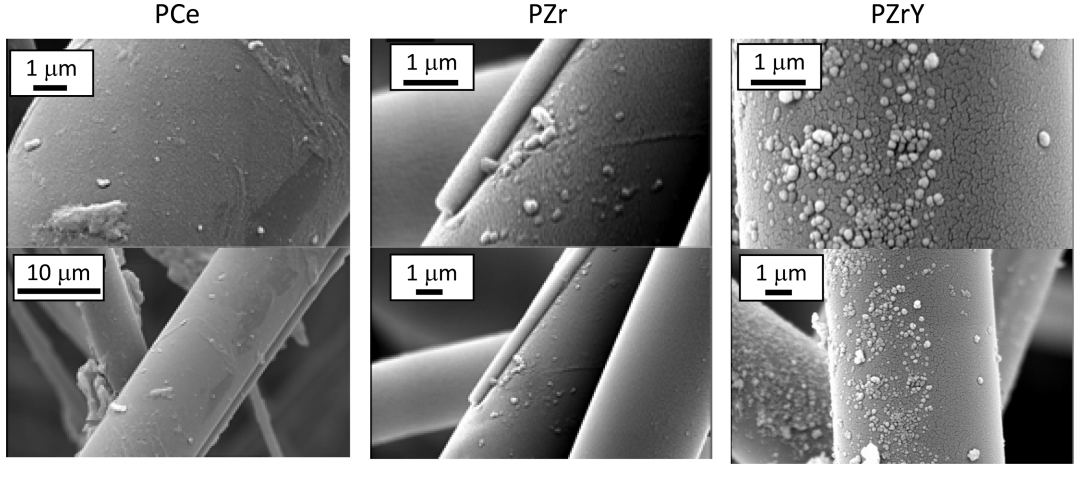

Figure 5. SEM micrographs of ceramic papers prepared with different binders.

dx.doi.org/10.1021/ie503154f | Ind. Eng. Chem. Res. 2014, 53, 17570−17579

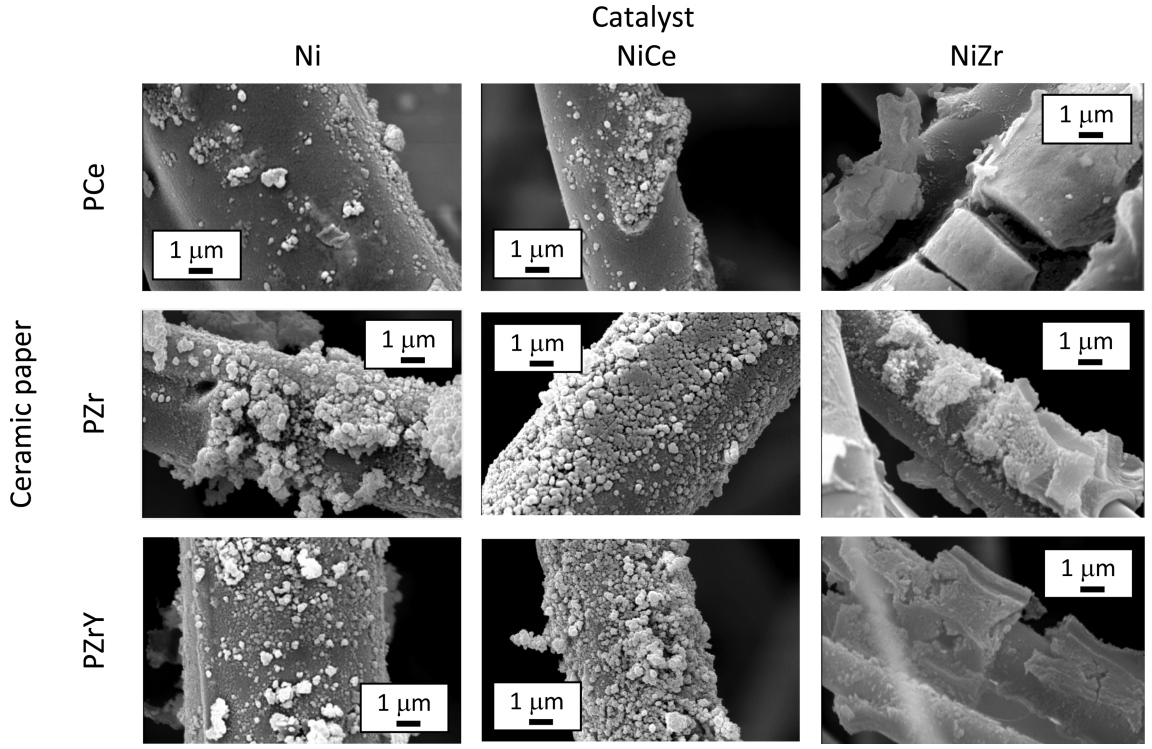

Figure 6. Morphology of the catalysts deposited on ceramic papers.

Table 2. EDX Results about Atomic Ratios Performed on the Catalytic Papers

	active phases					
	Ni		NiCe		NiZr	
ceramic papers	Ce/Ni	Zr/Ni	Ce/Ni	Zr/Ni	Ce/Ni	Zr/Ni
PCe	1.21 ± 0.24	–	1.45 ± 0.61	–	0.48 ± 0.33	0.21 ± 0.09
PZr	–	0.06 ± 0.03	0.14 ± 0.06	0.11 ± 0.05	–	0.16 ± 0.06
PZrY	–	0.07 ± 0.03	0.13 ± 0.01	0.03 ± 0.01	–	0.66 ± 0.12

produces a homogeneous coating along the fiber surface, with ceria nanoparticles completely covering them. The thickness of this layer, estimated from the SEM micrograph cross sections, was approximately 90−240 nm, with an average particle size (aggregates) of 30−70 nm.

The ceramic papers prepared with colloidal zirconia or yttria-stabilized zirconia also presented a uniform and well-distributed coverage of nanoparticles on the fibers. Similar to papers prepared with colloidal CeO_2, the thickness of the ZrO_2 binder film was around 80−220 nm in both cases, with average size of the aggregates between 20 and 80 nm. In addition, PZr and PZrY showed a smaller amount of binder aggregates placed in the fibers union. This could contribute to worse mechanical properties caused by a poorer contact between the ceramic fibers when compared with that of the PCe paper.

The catalytic papers presented a similar open structure after the addition of the active phases and the calcination step, suggesting that the impregnation procedure did not substantially modify the structure, porosity, and fiber arrangement (Figure 6).

Ni and NiCe catalyst particles were reasonably spread all over the structure and well-adhered to the binder-coated fibers, with average size of about 0.1−0.3 μm. The main shape was spherical, and the particles tended to form aggregates of 1−10 μm. Nevertheless, some differences could be noticed. The catalytic papers prepared from ceramic PZr and PZrY presented a distribution of the catalytic particles that was somewhat more even than that of papers prepared with ceramic PCe (Figure 6). The former papers (Ni and NiCe onto PZr and PZrY) showed particle groups that seemed to present greater order and compactness, which could partly explain the better catalytic performance of the mentioned systems, specifically NiCe−PZr and NiCe−PZrY.

In contrast, NiZr papers presented active phases organized in larger collections compared with those of Ni and NiCe systems. The catalytic components tended to form blocks with square forms and sizes larger than 1 μm.

Table 2 shows the atomic ratios present in the catalytic papers, obtained by EDX. Among the nonpromoted samples, those containing Zr and ZrY as binders show similar Zr/Ni ratios (0.06 and 0.07, respectively). However, the Ni−PZrY catalyst shows a productivity considerable higher than that of Ni−PZr, indicating that the binder is also participating in the reaction and that ZrY has a better behavior than Zr. When Ce is used as binder, the Ce/Ni ratio obtained is much higher than the Zr/Ni ratio, and the catalyst obtained presents the highest catalytic activity and selectivity of the group of the non-promoted samples. Thus, it is concluded that, for nonpromoted catalysts, Ce is a better binder than Zr and ZrY both for the mechanical properties and catalytic performance.

When the promoted catalytic papers were analyzed, the Ce/Ni atomic ratios for NiCe−PZr and NiCe−PZrY were similar

dx.doi.org/10.1021/ie503154f | Ind. Eng. Chem. Res. 2014, 53, 17570−17579

(0.14 and 0.13, respectively). Please note that in a previous study[25] we determined an optimal Ce/Ni atomic ratio of about 0.17, which gives higher ethylene productivity. The obtained Ce/Ni values were close to the nominal ratio of 0.17, suggesting a homogeneous spreading of the active phase and the employed promoter.

As could be expected, the NiCe−PCe system presented a higher Ce/Ni atomic ratio (1.45) and showed the poorest ethane conversion and ethylene selectivity among the cerium-promoted papers. When NiCe catalysts supported on PZr and PZrY are compared, the latter one shows a lower Zr/Ni ratio, and its productivity is the highest among all the catalysts studied in this work.

On the other hand, NiZr systems were the most selective catalysts but also the least active ones. The NiZr−PCe presented the best ethane conversion but the lowest selectivity by far among this group. The most efficient catalyst among the NiZr systems is NiZr−PZrY, demonstrating once again that the yttrium-doped zirconia possesses properties for the ODE reaction that are more adequate than those of pure zirconia. It was reported that the incorporation of yttrium to zirconia improved its oxygen transport properties, which could be useful for this reaction to some extent.[31] However, the lower catalytic performance of nickel−zirconia compared with nickel−ceria could be partly explained by the poorer oxygen storage capacity and lower oxygen transport capabilities of zirconia compared with those of ceria.[32]

3.3. Characterization of the Catalytic Active Phases. Figure 7 shows the XRD patterns of the catalytic papers.

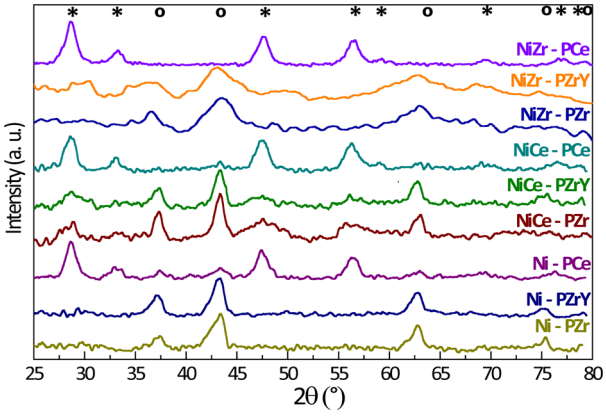

Figure 7. XRD diffraction patterns of catalytic ceramic papers. Symbols: O, NiO; *, CeO_2.

Characteristic peaks of NiO (JCPDS # 47-1049; 2θ = 37.3, 43.3, 62.9, 75.5, and 79.6°) were identified in the Ni-containing papers. The crystallite sizes of NiO were estimated to be 6.1, 9.1, and 6.8 nm for Ni−PCe, Ni−PZr and Ni−PZrY, respectively. Ni−PCe also showed the peaks corresponding to cerium oxide from the binder agent (JCPDS # 43-1002; 2θ = 28.6, 33.1, 47.5, 56.4, and 69.5°).

Cerium-promoted catalytic papers exhibited the presence of both nickel and cerium oxides with NiO crystallite sizes of 12.0, 8.7, and 6.3 nm for NiCe-PCe, NiCe-PZr, and NiCe-PZrY, respectively. If the sizes of NiO crystallites are compared with those corresponding to unpromoted formulations it can be established that the presence of cerium produces a decrease in the crystalline domains, as previously reported.[9] The exception was the NiCe−PCe in comparison with Ni−PCe probably because, in the former system, the nominal Ce/Ni ratio was higher than the optimal ratio (0.17) and this higher amount of cerium could produce a higher degree of oxide segregation, in agreement with their lower activity compared with that of NiCe−PZrY. Scherrer calculations indicate cerium oxide crystallite sizes of 5.9, 4.5, and 3.8 nm for NiCe−PCe, NiCe−PZr, and NiCe−PZrY, respectively. As can be seen, NiCe−PZrY presented the lowest crystallite sizes of both NiO and CeO_2, being the most active and the most selective system among the Ni and NiCe papers.

NiZr papers showed peaks corresponding to nickel oxide. The exception was NiZr−PCe, in which the NiO peaks could not be properly differentiated, probably because of their very low intensity. In this case, only ceria reflections were identified. The crystallite sizes of NiO were smaller than 3.0 nm for both NiZr−PZr and NiZr−PZrY. The zirconium oxide peaks under tetragonal (JCPDS entry 71-1282; 2θ main peaks at 29.8, 49.5, 50.1, and 59.4) or monoclinic (JCPDS entry 37-1484; 2θ main peaks at 28.2, 34.2, and 50.2°) forms were not found in any sample, suggesting that Zr was highly dispersed on the NiO matrix under an amorphous arrangement or formed a Ni−Zr−O solid solution because Ni^{2+} and Zr^{4+} presented similar ionic radii. A strong interaction between Ni and Zr was already observed by Wu et al.,[10] who reported that zirconium is able to enter into the nickel oxide structure.

Figure 8 shows the laser Raman spectra of the Ni-containing catalytic papers in which there appeared a broad and

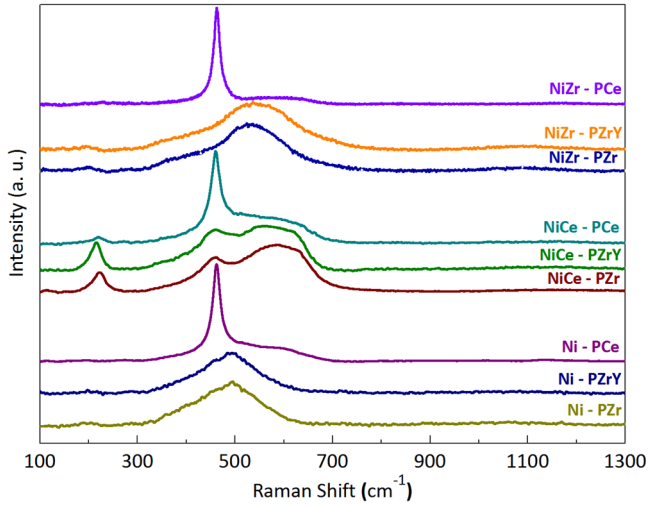

Figure 8. Raman spectra of the catalytic ceramic papers.

asymmetric band corresponding to the stretching of the Ni−O bond (first-order phonons), centered at ~500 cm^{-1}. In agreement with the X-ray diffraction patterns, this signal confirms the presence of bulk nickel oxide. Moreover, a significant shift in the frequency of the main signal was observed in Ni−PCe, indicating that the nickel−ceria interaction (ceria coming from the fiber coverage) occurred to some extent. The spectrum of this last catalytic paper displayed the cerium oxide typical band at 462 cm^{-1}.

The F2g vibration mode of cerium oxide corresponding to the fluorite-type structure of ceria presents a very sharp band[33] located at 465 cm^{-1}. Certainly, the Raman spectrum of the ceramic paper without active phases (PCe) presented this main band exactly at 465 cm^{-1} (not shown). However, the spectra of the Ce-containing catalysts (NiCe−PZr and NiCe−PZrY)

dx.doi.org/10.1021/ie503154f | Ind. Eng. Chem. Res. 2014, 53, 17570−17579

showed the above-mentioned characteristic signal, although shifted to lower frequencies (up to 10 cm^{-1}) (Figure 8). This fact suggests an evident distortion of the ceria structure. The NiCe−PCe system also presents this modification, but it is less pronounced, probably because of the high local concentration of cerium in the analyzed zone, which comes from the binder agent.

Furthermore, an extra band with different intensities located at ∼225 cm^{-1} and a shoulder at ∼625 cm^{-1}, associated with changes in the oxygen network, were clearly identified for the Ce-containing catalysts (NiCe−PZr and NiCe−PZrY).[18] Moreover, the Ni−O stretching band was notoriously shifted to higher frequencies (∼60−70 cm^{-1}) (Figure 8). These latter remarks confirm that the incorporation of Ni cations into the ceria lattice occurs to some extent, producing modifications in the lattice oxygen. This lattice alteration generates new species for the oxidative dehydrogenation of ethane and consequently produces some changes in the active sites. As a result, this group of catalysts presents the higher ethane conversion and ethylene productivity.

Crystalline domain size of CeO_2 was also estimated from the main signal of the corresponding Raman spectra, as proposed by Kanakaraju et al.[34] The calculations indicate sizes of 12.6, 1.4, and 1.1 nm for NiCe−PCe, NiCe−PZr, and NiCe−PZrY, respectively. These values are different than those estimated by the Scherrer equation, but they follow the same trend. The explanation of these differences was established elsewhere.[35]

Tetragonal zirconia characteristic Raman bands appear[36] at 148, 263, 325, 472, 608, and 640 cm^{-1}, whereas the monoclinic phase exhibits their corresponding bands[37] at 180, 188, 221, 380, 476, and 637 cm^{-1}. The spectra of NiZr papers present Raman bands similar to those of Ni-containing catalysts, but none of the typical zirconia bands was observed (Figure 8).

Crystalline zirconium oxide was not detected by XRD, probably because of a high dispersion. Moreover, amorphous oxide could not be seen either. In good agreement with those results, zirconium oxide was not identified by LRS because no extra signals corresponding to metal−oxygen bonds were observed. Even so, a comparison between Ni and NiZr spectra shows some differences. First, the Ni−O stretching band was notably shifted to higher frequencies (from 500 to 545 cm^{-1}), thus indicating a strong interaction between Ni and Zr and also suggesting changes in the NiO structure. A marked and well-defined shoulder corresponding to oxygen vacancies was observed at ∼400 cm^{-1}, confirming that zirconium was also incorporated into the nickel oxide structure. Moreover, the absence of ZrO_2 typical bands supports this hypothesis.

3.4. Mechanical Properties and Pressure Drop. The mechanical parameters that characterize the papers with respect to their flexibility and strength are the modulus of elasticity and tensile index, respectively. They were determined for the papers prepared using CeO_2, ZrO_2, and Y-ZrO_2 colloidal suspensions (PCe, PZr, and PZrY). Figure 9 shows the relationship between the applied load and total elongation of the papers, and Table 3 shows the average values obtained by testing different paper samples eight times.

Among the three samples studied, the PCe paper presented the highest tensile strength (maximum load, 6.17 N) but the lowest elasticity. Papers prepared from zirconia−yttria resulted in the least resistant structures, as can be observed in Figure 9.

On the other hand, the NiCe−PZrY and NiCe−PCe systems were selected to assess the catalytic bed permeability as a characteristic parameter that could indicate the resistance to the passage of gas flow. The functionality between total gaseous flow and pressure drop for both evaluated catalytic papers is presented in Figure 10. For comparison, values corresponding to the empty equipment are also shown. In this latter case, the equipment contained only a metallic mesh.

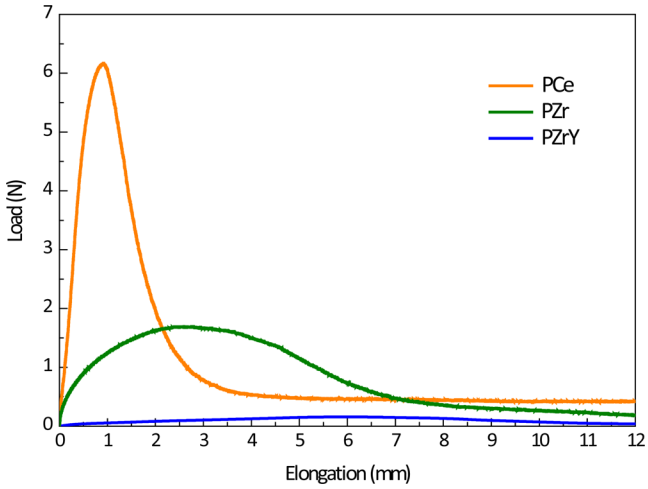

Figure 9. Mechanical properties: curves obtained for ceramic papers.

Table 3. Tensile Index and Modulus of Elasticity of the Prepared Ceramic Papers

ceramic paper	tensile index (Nm/g)	modulus of elasticity (MPa)
PZr	0.09 ± 0.008	0.56 ± 0.12
PZrY	ND[a]	ND[a]
PCe	0.22 ± 0.042	5.34 ± 1.78

[a]ND: not determined.

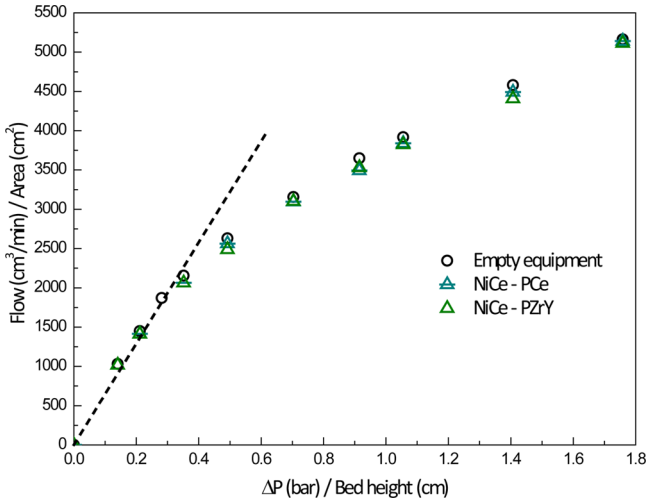

Figure 10. Paper permeation curves: air flow permeated as a function of the difference of applied pressure.

No significant differences between permeability of both NiCe catalytic papers (10 stacked paper discs) prepared with two different binder agents were observed. The final arrangement of the fibers covered with the binder and with the catalytic particles manifests very high permeability, close to that obtained for the empty enclosure with the stainless steel mesh used to contain the paper bed. After the tests, the loss of

dx.doi.org/10.1021/ie503154f | Ind. Eng. Chem. Res. 2014, 53, 17570−17579

catalyst particles was evaluated from weight measurements, and negligible quantities of catalytic papers were lost.

The very low pressure drop, i.e., the minimal resistance to the passage of a gas flow through the 10 stacked ceramic paper discs, demonstrates that this kind of open structure is a suitable substrate for the deposition of a catalytic formulation. In addition, it is a remarkable property if an industrial application is considered.

4. CONCLUSIONS

Flexible structured catalytic systems, active and selective for the oxidative dehydrogenation of ethane to produce ethylene, were obtained. The employed binder agents homogeneously covered the fiber surface, contributing with the double function of allowing a 3-D arrangement of ceramic fibers with adequate mechanical properties and permitting the subsequent anchoring of the selected catalytic formulation.

The prepared catalytic papers showed nickel oxide as the active phase (based on XRD, LRS, and EDX analyses). The incorporation of cerium or zirconium as promoters enhanced the catalytic properties compared with the corresponding unpromoted formulations. The first element, cerium, mainly produced an augmentation of ethane conversion while the latter, zirconium, led to a marked improvement in the selectivity to ethylene. Consequently, the global results indicated ethylene productivities of the promoted systems higher than those of the unpromoted samples, even at the very low W/F ratio analyzed. This was motivated by a modification of the active sites through the formation of solid solutions, Ni−Ce−O and Ni−Zr−O, as suggested by XRD and LRS analyses.

The binder agent, besides modifying the mechanical properties, also affected the catalytic performance through the alteration of the promoter/nickel atomic ratio. Mechanical properties were evaluated through the determination of the modulus of elasticity and tensile index, which allowed us to detect differences in the strength and flexibility of the prepared catalytic papers. In this sense, Nyacol ceria nanoparticles produced papers with better mechanical properties than those agglutinated with nanoparticles of either zirconia or zirconia−yttria.

AUTHOR INFORMATION

Corresponding Author

*Tel/FAX: +54-342-4536861. E-mail: emiro@fiq.unl.edu.ar.

Notes

The authors declare no competing financial interest.

ACKNOWLEDGMENTS

The authors acknowledge the financial support received from ANPCyT, CONICET, SECTEI Santa Fe, and UNL. Thanks are also given to Elsa Grimaldi for the English language editing and to Delfina Terzaghi for her help in the experimental work.

REFERENCES

(1) Cavani, F.; Ballarini, N.; Cericola, A. Oxidative dehydrogenation of ethane and propane: How far from commercial implementation? *Catal. Today* **2007**, *127*, 113.

(2) Schuurman, Y.; Ducarme, V.; Chen, T.; Li, W.; Mirodatos, C.; Martin, G. A. Low temperature oxidative dehydrogenation of ethane over catalysts based on group VIII metals. *Appl. Catal., A* **1997**, *163*, 227.

(3) Zhang, X.; Liu, J.; Jing, Y.; Xie, Y. Support effects on the catalytic behavior of NiO/Al_2O_3 for oxidative dehydrogenation of ethane to ethylene. *Appl. Catal., A* **2003**, *240*, 143.

(4) Nakamura, K. I.; Miyake, T.; Konishi, T.; Suzuki, T. Oxidative dehydrogenation of ethane to ethylene over NiO loaded on high surface area MgO. *J. Mol. Catal. A: Chem.* **2006**, *260*, 144.

(5) Heracleous, E.; Lee, A. F.; Wilson, K.; Lemonidou, A. A. Investigation of Ni-based alumina-supported catalysts for the oxidative dehydrogenation of ethane to ethylene: Structural characterization and reactivity studies. *J. Catal.* **2005**, *231*, 159.

(6) Heracleous, E.; Lemonidou, A. A. Ni−Me−O mixed metal oxides for the effective oxidative dehydrogenation of ethane to ethylene−Effect of promoting metal Me. *J. Catal.* **2010**, *270*, 67.

(7) Solsona, B.; Ivars, F.; Dejoz, A.; Concepción, P.; Vázquez, M. I.; López Nieto, J. M. Supported Ni−W−O Mixed oxides as selective catalysts for the oxidative dehydrogenation of ethane. *Top. Catal.* **2009**, *52*, 751.

(8) Solsona, B.; López Nieto, J. M.; Concepción, P.; Dejoz, A.; Ivars, F.; Vázquez, M. I. Oxidative dehydrogenation of ethane over Ni−W−O mixed metal oxide catalysts. *J. Catal.* **2011**, *280*, 28.

(9) Solsona, B.; Concepción, P.; Hernández, S.; Demicol, B.; López Nieto, J. M. Oxidative dehydrogenation of ethane over $NiO-CeO_2$ mixed oxides catalysts. *Catal. Today* **2012**, *180*, 51.

(10) Wu, Y.; Gao, J.; He, Y.; Wu, T. Preparation and characterization of Ni−Zr−O nanoparticles and its catalytic behavior for ethane oxidative dehydrogenation. *Appl. Surf. Sc.* **2012**, *258*, 4922.

(11) Bortolozzi, J. P.; Gutierrez, L. B.; Ulla, M. A. Synthesis of Ni/Al_2O_3 and $Ni-Co/Al_2O_3$ coatings onto AISI 314 foams and their catalytic application for the oxidative dehydrogenation of ethane. *Appl. Catal., A* **2013**, *452*, 179.

(12) Bortolozzi, J. P.; Gutierrez, L. B.; Ulla, M. A. Comparison of Ni and $Ni-Ce/Al_2O_3$ catalysts in granulated and structured forms: Their possible use in the oxidative dehydrogenation of ethane reaction. *Chem. Eng. J. (Amsterdam, Neth.)* **2014**, *246*, 343.

(13) Bortolozzi, J. P.; Gutierrez, L. B.; Ulla, M. A. Efficient structured catalysts for ethylene production through the ODE reaction: Ni and Ni−Ce on ceramic foams. *Catal. Commun.* **2014**, *43*, 197.

(14) Banús, E. D.; Ulla, M. A.; Galván, M. V.; Zanuttini, M. A.; Milt, V. G.; Miró, E. E. Catalytic ceramic paper for the combustion of diesel soot. *Catal. Commun.* **2010**, *12*, 46.

(15) Tuler, F. E.; Banús, E. D.; Zanuttini, M. A.; Miró, E. E.; Milt, V. G. Ceramic papers as flexible structures for the development of novel diesel soot combustion catalysts. *Chem. Eng. J. (Amsterdam, Neth.)* **2014**, *246*, 287.

(16) Shiratori, Y.; Quang-Tuyen, T.; Umemura, Y.; Kitaoka, T.; Sasaki, K. Paper-structured catalyst for the steam reforming of biodiesel fuel. *Int. J. Hydrogen Energy* **2013**, *38*, 11278.

(17) Miura, S.; Umemura, Y.; Shiratori, Y.; Kitaoka, T. In situ synthesis of Ni/MgO catalysts on inorganic paper-like matrix for methane steam reforming. *Chem. Eng. J. (Amsterdam, Neth.)* **2013**, *229*, 515.

(18) Shiratori, Y.; Ogura, T.; Nakajima, H.; Sakamoto, M.; Takahashi, Y.; Wakita, Y.; Kitaoka, T.; Kazunari, S. Study on paper-structured catalyst for direct internal reforming SOFC fueled by the mixture of CH_4 and CO_2. *Int. J. Hydrogen Energy* **2013**, *38*, 10542.

(19) Cecchini, J. P.; Serra, R. M.; Barrientos, C. M.; Ulla, M. A.; Galván, M. V.; Milt, V. G. Ceramic papers containing Y zeolite for toluene removal. *Microporous Mesoporous Mater.* **2011**, *145*, 51.

(20) Koga, H.; Kitaoka, H. One-step synthesis of gold nanocatalysts on a microstructured paper matrix for the reduction of 4-nitrophenol. *Chem. Eng. J. (Amsterdam, Neth.)* **2011**, *168*, 420.

(21) Koga, H.; Umemura, Y.; Kitaoka, T. Design of catalyst layers by using paper-like fiber/metal nanocatalyst composites for efficient NO_X reduction. *Composites, Part B* **2011**, *42*, 1108.

(22) Kwon, H. J.; Kim, Y.; Nam, I. S.; Jung, S. M.; Lee, J. H. The hydrothermal stability of paper-like ceramic fiber and conventional honeycomb-type cordierite substrates washcoated with Cu-MFI and V_2O_5/TiO_2 catalysts for the selective reduction of NO_X by NH_3. *Top. Catal.* **2010**, *53*, 439.

(23) Ishihara, H.; Koga, H.; Kitaoka, T.; Wariishi, H.; Tomoda, A.; Suzuki, R. Paper-structured catalyst for catalytic removal from combustion exhaust gas. *Chem. Eng. Sci.* **2010**, *65*, 208.
(24) Koga, H.; Kitaoka, T.; Nakamura, M.; Wariishi, H. Paper-structured catalyst for catalytic NO_X removal from combustion exhaust gas. *J. Mater. Sci.* **2009**, *44*, 5836.
(25) Bortolozzi, J. P.; Banús, E. D.; Terzaghi, D.; Gutierrez, L. B.; Milt, V. G.; Ulla, M. A. Novel catalytic ceramic papers applied to oxidative dehydrogenation of ethane. *Catal. Today* **2013**, *216*, 24.
(26) Ichiura, H.; Kubota, Y.; Wu, Z.; Tanaka, H. Preparation of zeolite sheets using a papermaking technique: Part I Dual polymer system for high retention of stock components. *J. Mater. Sci.* **2001**, *36*, 913.
(27) Ichiura, H.; Okamura, N.; Kitaoka, T.; Tanaka, H. Preparation of zeolite sheet using a papermaking technique: Part II The strength of zeolite sheet and its hygroscopic characteristics. *J. Mater. Sci.* **2001**, *36*, 4921.
(28) Pan, Q.; Peng, J.; Sun, T.; Gao, D.; Wang, S.; Wang, S. CO_2 methanation on $NiCe_{0.5}Zr_{0.5}O_2$ catalysts for the production of synthetic natural gas. *Fuel Process. Technol.* **2014**, *123*, 166.
(29) Atribak, I.; Guillén-Hurtado, N.; Bueno-López, A.; García-García, A. Influence of the physico-chemical properties of CeO_2−ZrO_2 mixed oxides on the catalytic oxidation of NO to NO_2. *Appl. Surf. Sci.* **2010**, *256*, 7706.
(30) Väliheikki, A.; Petallidou, K. C.; Kalamaras, C. M.; Kolli, T.; Huuhtanen, M.; Maunula, T.; Keiski, R. L.; Efstathiou, A. M. Selective catalytic reduction of NO_x by hydrogen (H_2-SCR) on WO_x-promoted $Ce_zZr_{1-z}O_2$ solids. *Appl. Catal., B* **2014**, *156*−*157*, 72.
(31) Zhu, J.; van Ommen, J. G.; Lefferts, L. Partial oxidation of methane by O_2 and N_2O to syngas over yttrium-stabilized ZrO_2. *Catal. Today* **2006**, *112*, 82.
(32) Pakulska, M. M.; Grgicak, C. M.; Giorgi, J. B. The effect of metal and support particle size on NiO/CeO_2 and NiO/ZrO_2 catalyst activity in complete methane oxidation. *Appl. Catal., A* **2007**, *332*, 124.
(33) Martínez−Arias, A.; Fernández−Garcías, M.; Salamanca, L. N.; Valenzuela, R. X.; Conesa, J. C.; Soria, J. Structural and redox properties of ceria in alumina-supported ceria catalyst supports. *J. Phys. Chem. B* **2000**, *104*, 4038.
(34) Kanakaraju, S.; Mohan, S.; Sood, A. K. Optical and structural properties of reactive ion beam sputter deposited CeO_2 films. *Thin Solid Films* **1997**, *305*, 191.
(35) Bourja, L.; Bakiz, B.; Benlhachemi, A.; Ezahri, M.; Villain, S.; Favotto, C.; Valmalette, J. C.; Gavarri, J. R. Structural modifications of nanostructured ceria CeO_2,xH_2O during dehydration process. *Powder Technol.* **2012**, *215*−*216*, 66.
(36) Sohn, J. R.; Doh, I. J.; Pae, Y. I. Spectroscopic study of V_2O_5 supported on zirconia and modified with WO_3. *Langmuir* **2002**, *18*, 6280.
(37) Scheithauer, M.; Grasselli, R. K.; Knözinger, H. Genesis and structure of WO_x/ZrO_2 solid acid catalysts. *Langmuir* **1998**, *14*, 3019.